

HIGH RESOLUTION LASER SPECTROSCOPY OF ODD-PARITY BARIUM RYDBERG STATES POPULATED BY FORBIDDEN ATOMIC TRANSITIONS

H. Rinneberg and J. Neukammer

Inst. f. Atom- und Festkörperphysik, FU Berlin, 1000 Berlin 33, F.R.G.

Résumé - Nous avons peuplé des niveaux de Rydberg impairs du baryum par la méthode d'excitation laser à deux étages en utilisant des transitions M1-E1 et E2-E1 à partir du niveau fondamental $6s^2 \ ^1S_0$. A l'aide de deux lasers à colorant en anneau et d'une détection thermo-ionique, nous avons mesuré les spectres sans largeur Doppler des niveaux de Rydberg $6snp \ ^1,3P$ et $6snf \ ^1,3F$ en obtenant des rapports signal/bruit excellents. Nous avons étudié systématiquement la structure hyperfine des états de Rydberg $6snp \ ^1P_1$. Entre $n=20$ et $n=23$, nous observons une résonance due au mélange singulet-triplet produit par l'interaction de configuration avec le niveau $5d8p \ ^1P_1$ perturbateur proche de la limite d'ionisation. Nos résultats sont en désaccord avec une analyse existante de cette série à l'aide de la méthode du défaut quantique à plusieurs voies. Les mélanges singulet-triplet des séries de niveaux de Rydberg $6snp \ ^1P_1$ et $6snd \ ^1D_2$ sont comparés.

Abstract - Odd-parity barium Rydberg states have been populated by stepwise excitation via M1-E1 and E2-E1 transitions, starting from the $6s^2 \ ^1S_0$ ground state. Using two cw dye ring lasers and employing thermionic detection, Doppler-free spectra of $6snp \ ^1,3P$ and $6snf \ ^1,3F$ Rydberg states have been recorded with excellent signal/noise ratios. A systematic study of the hyperfine structure of $6snp \ ^1P_1$ Rydberg states has been carried out. Between $n=20$ and $n=23$ a resonance in singlet-triplet mixing occurs caused by configuration interaction with the $5d8p \ ^1P_1$ perturbing state, located close to the first ionization limit. Our results are in disagreement with an existing multichannel quantum defect analysis of this series. The singlet-triplet mixing of $6snp \ ^1P_1$ and $6snd \ ^1D_2$ Rydberg series is compared.

1. INTRODUCTION

High resolution laser spectroscopy of atomic Rydberg states has been actively pursued by several research groups within the past five years. Besides the alkalis Rb /1/ and Cs /2/ the two-electron systems /3/ Ca /4/, Sr /5/, Ba /6,7/, and Yb /8/ have received a great deal of attention. Recently such measurements have been extended to atoms with three valence electrons (In) as well /9/. Detailed information concerning the electronic structure of Rydberg states of two-electron systems has been deduced from measured g-factors /10/, hyperfine structures /3-8/

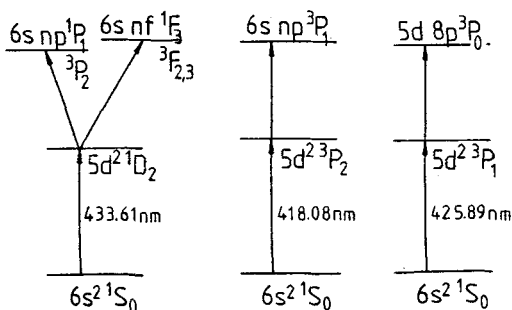
and isotope shifts /11,12/. For example, the hyperfine structures of $msnd\ ^1D_2$ and 3D_2 Rydberg states of Ca ($m=4$), Sr ($m=5$), and Ba ($m=6$) were used to sensitively monitor singlet-triplet mixing caused by configuration interactions of these Rydberg series with doubly excited perturbing states.

In most experiments Rydberg states were reached by two-photon absorption starting from the atomic ground states. For stepwise excitation via resonant E1-E1 transitions moderate powers (0.01 - 0.1 W) of the cw dye laser radiations employed are sufficient to populate the Rydberg states, because of the large oscillator strengths connected with resonant dipole transitions. Furthermore, purely optical techniques /13/ may be used to detect Rydberg atoms. For off-resonant E1-E1 transitions, however, the low oscillator strength requires considerably larger power densities of the laser radiation as well as sensitive detection schemes. These conditions can be met using cw dye ring lasers with output powers of typically 0.1 - 1 W and thermionic diodes which are extremely sensitive detectors for Rydberg states. In this way Rydberg series of the same parity as the ground state have been studied up to now.

Starting from the atomic ground state an odd number of electric dipole transitions is required to reach Rydberg states of opposite parity. For example, Garton and Tomkins /14/ employed classical optical spectroscopy to study the $6snp\ ^1P_1$ Rydberg series of Ba, populated by a one-photon transition from the $6s^2\ ^1S_0$ ground state. Subsequently Armstrong et al. /15/ excited $6snp\ ^1P_1$ and $6snp\ ^3P_{1,2}$ states via the cascades $6s^2\ ^1S_0 \rightarrow 6s6p\ ^3P_1 \rightarrow 6s7s\ ^1S_0, (^3S_1) \rightarrow 6snp\ ^1,^3P$, using three pulsed dye lasers. In principle such excitation schemes can be employed for high resolution studies as well. However, since narrow-band tunable UV laser radiation of sufficiently short wavelength is not available yet, one-photon excitations of odd parity Ba Rydberg states have to proceed from metastable excited states. In this way Elie and Hogervorst /16/ measured hyperfine structures and isotope shifts of $6snf\ ^3F$ Rydberg states ($20 \leq n \leq 50$) starting from the $5d6s\ ^3D_{1,2}$ metastable states. However, the sensitivity was insufficient to record high resolution spectra of $6snp\ ^1,^3P$ and $6snf\ ^1F_3$ Rydberg series. In this paper we report on an elegant technique to populate odd-parity Rydberg states of alkaline-earth atoms by two-photon excitation via resonant M1-E1 and E2-E1 transitions. For demonstration we have measured isotope shifts and hyperfine structures of $6snp\ ^1,^3P$ and $6snf\ ^1,^3F$ Rydberg states of barium. Starting from the $6s^2\ ^1S_0$ ground state, Rydberg states were reached via $5d^2\ ^3P_1, ^3P_2$ and 1D_2 intermediate

Fig. 1 - Two-step excitation of $6snp$ and $6snf$ barium Rydberg states via M1-E1 and E2-E1 transitions.

levels (cf. Fig. 1). Similar to off-resonant E1-E1 transitions, the low oscillator strength of forbidden atomic transitions can be counterbalanced by the high output powers of cw dye ring lasers and the sensitivity of thermionic detection.



2. EXPERIMENTAL

Two stabilized cw dye ring lasers (Fig. 2) with a bandwidth of about 1 MHz were used in our experiment. The first ring laser, operating between 417 nm and 460 nm, provided sufficient intensity (0.1 - 0.3 W) to induce the M1 or E2 transitions $6s^2 1S_0 \rightarrow 5d^2$ at $\lambda_1 = 425.9$ nm (3P_1), $\lambda_1 = 418.1$ nm (3P_2) and $\lambda_1 = 433.6$ nm (1D_2). The second dye ring laser could be tuned between 520 and 615 nm and excited the atoms from the intermediate to the final Rydberg states (cf.

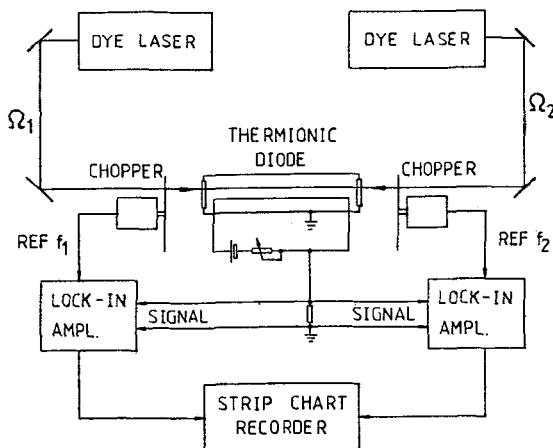


Fig. 2 - Experimental setup

Fig. 1). The wavelengths

were measured using a commercial wavemeter. A

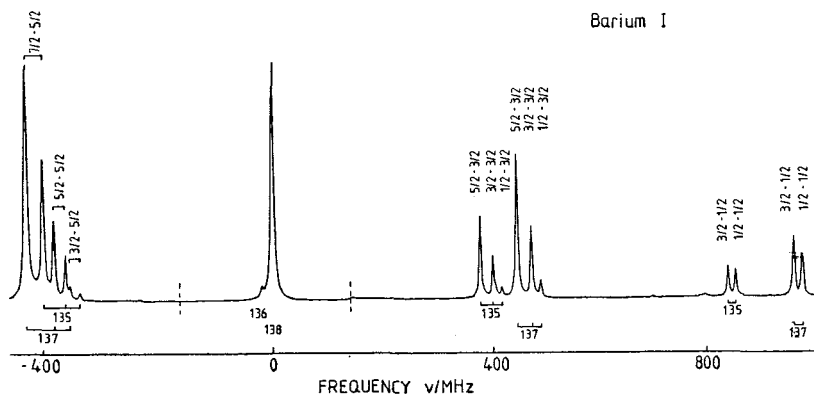
marker cavity with a free spectral range of 149.7 MHz provided the necessary frequency calibration. The beams of both dye lasers were superimposed and co- or counterpropagated through a stainless steel pipe filled with Ba and heated to about 700°C . Both laser beams were linearly and parallel polarized. To prevent coating of the windows, the oven was filled with 50 mTorr of Ar buffer gas. For thermionic detection the stainless steel pipe was taken as anode while a 5-mil tungsten wire running along its center served as cathode. The cathode was heated

to red glow by a dc current of about 1 A. The diode was operated with a potential difference of about 1 V between the electrodes. The voltage drop across a 50 k Ω load resistor was fed into two lock-in amplifiers. Two choppers, modulating the intensity of the first and second laser beam at a rate of $f_1 = 1.6$ kHz and $f_2 = 73$ Hz, respectively, served as references for the lock-in amplifiers. Due to velocity selective optical pumping /17/ two-step excitation with co- or counter-propagating laser beams results in Doppler-free spectra. They were recorded by scanning the frequency $\Omega_2/2\pi$ of the second laser across the upper atomic transitions, while the wavelength λ_1 of the first laser was kept fixed at an arbitrary position within the Doppler contour of the particular forbidden atomic transition. Although Doppler-free signals corresponding to excitations to the (final) Rydberg states were observed at either modulation frequency, detection at f_2 yielded superior signal/noise ratios. The modulation of the first laser beam at the frequency f_1 mainly served to observe the Doppler-broadened first transitions $6s^2\ ^1S_0 \rightarrow 5d^2\ ^1D_2, ^3P_1$ and 3P_2 employing thermionic detection. Since these atomic states are located about $19\ 000\ \text{cm}^{-1}$ below the first ionization limit, the ions are produced most likely by photoionization of these states due to the absorption of another blue photon. Contrary to highly excited Rydberg states, collisional ionization can be ruled out for these low lying levels. Thermionic detection of the Doppler-broadened M1 or E2 transitions greatly facilitates the search for the Doppler-free transitions to the Rydberg states reported in this paper.

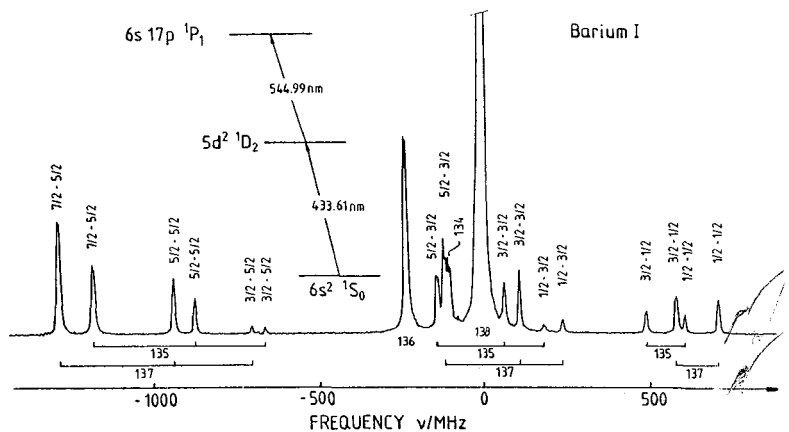
In Fig. 3 Doppler-free spectra of the $6s17p\ ^1P_1$ Rydberg state are shown, recorded with counterrunning (Fig. 3a) or copropagating (Fig. 3b) laser beams. Besides the isotope shifts of the even isotopes $^{134}, ^{136}, ^{138}\text{Ba}$ the spectra clearly exhibit the hyperfine structures of the odd isotopes $^{135}, ^{137}\text{Ba}$ ($I=3/2$). The hyperfine structures of the intermediate ($5d^2\ ^1D_2$) and final state ($6s17p\ ^1P_1$) appear in the spectra. Therefore the hyperfine components are labelled $F_i - F_f$ according to the hyperfine levels of the intermediate and final state involved in the two-step excitation. Generally, the contribution of the intermediate state to the observed hyperfine splittings depends on the geometry chosen. For counterpropagating laser beams, the hyperfine structure of the intermediate level is reduced by a factor $(v_2 - v_1)/v_1$ (cf. Fig. 3a) while hyperfine splittings enlarged by the factor $(v_2 + v_1)/v_1$ are recorded for copropagating beams (see Fig. 3b). Also, both optical transitions add to the measured isotope shifts, with the contribution of the first transition weighed by the factors $-v_2/v_1$ and $+v_2/v_1$ for co-

Fig. 3 -
Spectrum of
the Ba $6s17p$
 $1p_1$ Rydberg
state ex-
cited by

a) counter-
propagating
laser beams

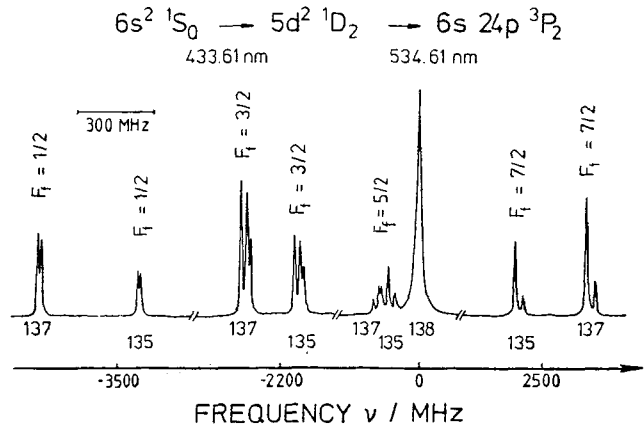


b) copropa-
gating laser
beams



and counterpropagating laser beams, respectively. Since the transition $6s^2 \rightarrow 5d^2$ corresponds to a decrease, the excitation $5d^2 \rightarrow 6snp$ to an increase in electron density at the nucleus, the isotope shifts of both transitions are of opposite sign. Hence the contributions of the first and second transition to the measured isotope shifts add for copropagating but almost cancel for counterpropagating laser beams. This is clearly exhibited in Figs. 3a and b. The influence of the geometry on the measured hyperfine splittings and isotope shifts can be easily understood. At fixed frequency the first laser beam excites different velocity ensembles to the intermediate state, Doppler-tuned to the various hyperfine components of the first optical transition. For a counterpropagating second laser beam these velocity ensembles experience different Doppler shifts and hence a different frequency of the second laser is required to excite a particular velocity ensemble to the same final state.

Fig. 4 - High resolution spectrum of the $6s24p^3P_2$ Ba Rydberg state.



Compared to the $1P_1$ Rydberg series, transitions to $6snp^3P$ Rydberg states are of considerably lower oscillator strengths with transitions to the $3P_2$ fine structure

components being strongest /15/. Fig. 4 displays the Doppler-free spectrum of the $6s24p^3P_2$ Rydberg state, recorded with counterrunning laser beams. Due to configuration interaction with a close-lying $5d8p^3P_2$ perturber, transitions to this Rydberg state were found to be exceptionally strong. Generally the hyperfine structure of $6snp^3P_1$ Rydberg states escaped detection choosing the $5d^2 1D_2$ state as intermediate level. However this Rydberg series could be effectively populated via the $5d^2 3P_2$ fine structure component, although the quadrupole transition $6s^2 1S_0 \rightarrow 5d^2 3P_2$ is nominally spin-forbidden. As an example, the Doppler-free spectrum of the $6s17p^3P_1$ state is displayed in Fig. 5. In order to reach highly excited atomic states with $J=0$ by two-step excitation, the magnetic dipole transition $6s^2 1S_0 \rightarrow 5d^2 3P_1$ was selected. The Doppler-free spectrum of the $5d8p^3P_0$ level is shown in Fig. 6. This state is thought to perturb the $6snp^3P_0$ Rydberg series /15/ which has not been observed up to now. Since $J=0$, the

Fig. 5 - Doppler-free spectrum of the $6s17p^3P_1$ Ba Rydberg state

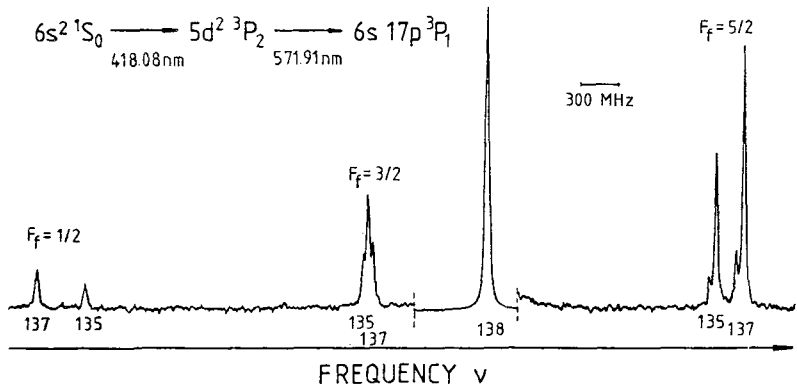


Fig. 6 - Doppler-free spectrum of the $5d8p\ ^3P_0$ perturbing state of Ba^0 populated by M1-E1 transitions

splittings of the $F_f=3/2$ components of $^{135,137}\text{Ba}$ (cf. Fig. 6) are entirely due to the hyperfine structure of the $5d^2\ ^3P_1$ intermediate level.

Apart from the $6snp\ ^{1,3}P$ Rydberg series, $6snf\ ^3F_2$, 3F_3 ($10 \leq n \leq 21$) and $6snf\ ^1F_3$ ($10 \leq n \leq 40$) Rydberg states have been

studied in detail. Choosing the $5d^2\ ^1D_2$ fine structure component as intermediate level, excitations to $6snf$ Rydberg states are favored over transitions to the $6snp$ series. For example, signals of up to 1 V corresponding to signal/noise ratios of about 1000 for the most abundant isotope ^{138}Ba , were observed for $6snf\ ^1F_3$ Rydberg states. The spectrum of the $6s26f\ ^1F_3$ Rydberg level, shown in Fig. 7, has been recorded with copropagating laser beams.

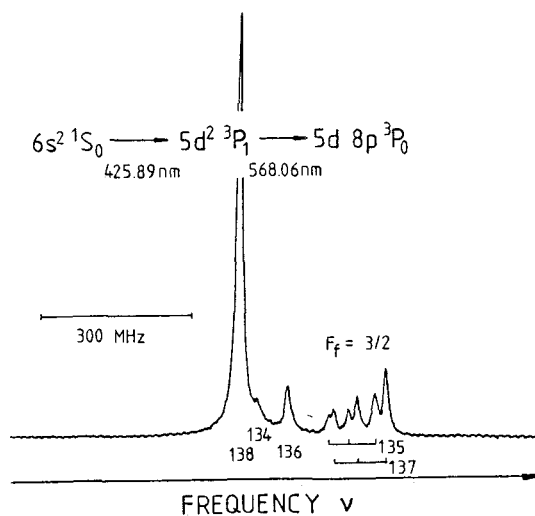
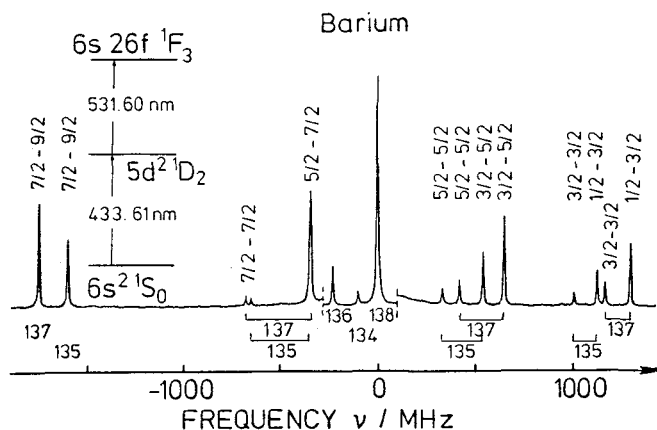


Fig. 7 - High resolution spectrum of the $6s26f\ ^1F_3$ Ba Rydberg state



III. DISCUSSION

The $msnl$ Rydberg series of alkaline-earth elements are strongly perturbed due to Coulomb interaction with doubly excited configurations. Barium is notorious for the large number of perturbing states, pre-

dominantly of $5dn'l'$ configuration. By studying barium Rydberg series employing high resolution laser spectroscopy we aim at determining the wavefunctions of these states. Although isotope shifts can be used to derive the amount of admixture of perturbing configurations into the $6snl$ Rydberg states quantitatively /11,12/, in the following we restrict ourselves to a discussion of the hyperfine structures of $6snp$ 1P_1 and $6snd$ 1D_2 Rydberg series.

For Rydberg states of pure $6snp$ or $6snd$ configuration spin-orbit interaction of the Rydberg electron

$$H_{so} = \xi_{nl} \vec{s}_2 \cdot \vec{l}_2 \quad (1)$$

causes singlet and triplet states to mix. Using intermediate coupling the wavefunctions of Rydberg states of pure $6snl$ ($l=1,2$) configuration are expressed as

$$\overline{|6snl \ ^1L_1\rangle} = \Lambda_{so} \overline{|6snl \ ^1L_1\rangle} + \Omega_{so} \overline{|6snl \ ^3L_1\rangle} \quad (2)$$

$$\overline{|6snl \ ^3L_1\rangle} = -\Omega_{so} \overline{|6snl \ ^1L_1\rangle} + \Lambda_{so} \overline{|6snl \ ^3L_1\rangle} \quad (3)$$

with $\Omega_{so}^2 + \Lambda_{so}^2 = 1$. The wavefunctions have been expanded in terms of pure configuration, exactly SL-coupled basis vectors indicated by the long horizontal bars. Also, on the left hand side of Eqs.(2,3), the pure $6snl$ character of the wavefunctions is indicated. Using second order perturbation theory the triplet amplitude Ω_{so} can be expressed in terms of the spin-orbit coupling constant and the singlet-triplet separation, e.g.

$$\Omega_{so} (^1D_2) = \sqrt{3/2} \xi_{nd} / \Delta E_{ST} \quad (4)$$

where

$$\Delta E_{ST} = E(\overline{|6snd \ ^1D_2\rangle}) - E(\overline{|6snd \ ^3D_2\rangle}) \quad (5)$$

Since for Rydberg states of pure $6snd$ configuration both ξ_{nl} and ΔE_{ST} decrease proportional to n^{*-3} , n^* being the effective quantum number, Ω_{so} is expected to be essentially independent of the principal quantum number n .

Because of singlet-triplet mixing, the strong Fermi-contact interaction of the $6s$ valence electron with the nuclear magnetic moments of $^{135,137}\text{Ba}$ results in well-resolved hyperfine structures of $6snp$ 1P_1

and $6snd\ ^1D_2$ Rydberg states. Neglecting any direct interaction of the Rydberg electron with the nuclear magnetic moment, the Hamiltonian describing the hyperfine interaction is given by

$$H_{hf} = a_{6s} \vec{s}_1 \cdot \vec{I} . \quad (6)$$

Generally, taking the free ion value for a_{6s} represents a good approximation. With the aid of Eqs.(2,6), the hyperfine splitting factors A corresponding to singlet states of pure $6snl$ ($l=1,2$) configuration are calculated to first order to be

$$A(^1L_1) = \frac{a_{6s}}{2l(l+1)} \{ \Omega_{so}^2(^1L_1) - 2\sqrt{l(l+1)} \Omega_{so}(^1L_1) \Lambda_{so}(^1L_1) \} \quad (7)$$

Eq.(7) is valid, provided the hyperfine coupling constant a_{6s} is considerably smaller than the singlet-triplet separation $|\Delta E_{ST}|$. For $|a_{6s}| \sim |\Delta E_{ST}|$ off-diagonal elements of the Hamiltonian H_{hf} between the 1P_1 and $^3P_{0,1,2}$ or 1D_2 and $^3D_{1,2,3}$ fine structure components may lead to dramatic shifts of the individual hyperfine components and a description of the hyperfine structure by a splitting factor A may no longer be possible. Provided the singlet-triplet separation is known from experiment, however, the hyperfine-induced mixing of the true wavefunctions of the fine structure components as well as the displacements of the individual hyperfine components can be calculated exactly by diagonalization.

In Figs. (8,9) the position of the hyperfine components F_f of the $6snp\ ^1P_1$ and $6snd\ ^1D_2$ Rydberg states have been plotted versus n , respectively. The variation of the hyperfine splittings with principal quantum number n reflects changes in the coupling of both valence electrons. As was mentioned above, pure $6snl$ Rydberg states are predominantly SL-coupled and the singlet-triplet mixing caused by spin-orbit interaction is almost independent of n . However, strong configuration interactions with doubly excited $5dn'l'$ states which are generally best described by jj -coupling, may result in a complete breakdown of SL-coupling. For example the dramatic resonance-like variation of the hyperfine splitting of $6snd\ ^1D_2$ Rydberg states (cf. Fig. 9) observed for principal quantum numbers ranging between 20 and 35 is caused by the configuration interaction of this Rydberg series with the $5d7d\ ^1D_2$ perturber, located between $n=26$ and $n=27$. A similar resonance occurs for $6snp\ ^1P_1$ states between $n=18$ and $n=30$. However, at $n=21$ and $n=22$ strong hyperfine-induced mixing of the nearly degenerate fine structure components 1P_1 and 3P_2 result in a repulsion of hyperfine components with the same principal quantum number F_f , partially masking the

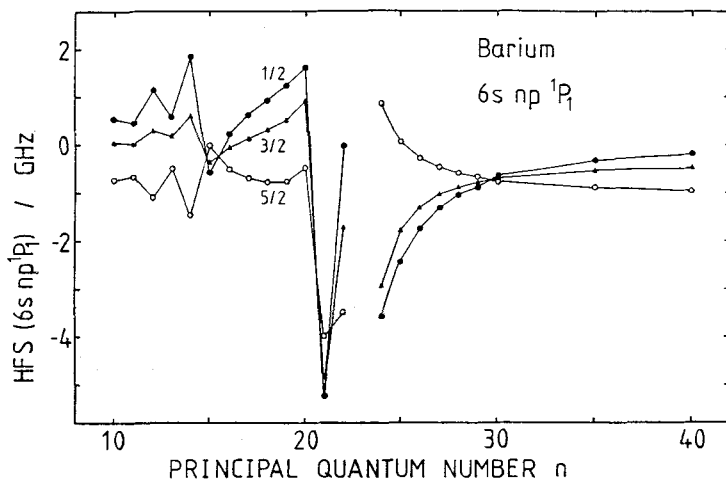
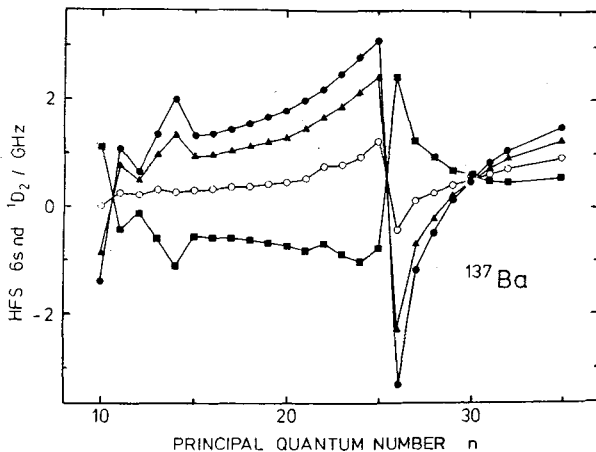


Fig. 8 - Positions of the hyperfine components $F_f = 1/2, 3/2,$ and $5/2$ of ^{137}Ba of $6snp\ ^1P_1$ Rydberg states. The frequencies are measured relative to ^{138}Ba . The data have been corrected for the isotope shifts of the quadrupole transition $6s^2\ ^1S_0 \rightarrow 5d^2\ ^1D_2$ as well as for the hyperfine splitting of the intermediate state. The term values and designation of the Rydberg states as $6snp\ ^1P_1$ levels were taken from Ref. 15.

Fig. 9 - Positions of the hyperfine components $F_f = 1/2$ (\bullet), $3/2$ (\blacktriangle), $5/2^f$ (\circ), and $7/2$ (\blacksquare) of ^{137}Ba of $6snd\ ^1D_2$ Rydberg states. The frequencies are measured relative to ^{138}Ba . The data have been corrected for the hyperfine splitting of the intermediate $6s6p\ ^1P_1$ level. The isotope shifts of the first transition $6s^2\ ^1S_0 \rightarrow 6s6p\ ^1P_1$, still contained in the data, result in a vertical displacement virtually independent of n .



resonance-like variation of the hyperfine structure of the 1P_1 series. Furthermore, the oscillator strength of the transition $5d^2\ ^1D_2 \rightarrow 6snp\ ^1P_1$ shows a pronounced minimum around $n=23$. Because the transition probability drops by about two orders of magnitude the hyperfine structure of the $6s23p\ ^1P_1$ state could not be observed. The decrease in oscillator strength around $n=23$ is explained as Fano-minimum of the $5d8p\ ^1P_1$ perturber.

Besides the configuration interactions of the $5d7d\ ^1D_2$ and $5d8p\ ^1P_1$ perturbing levels influencing a larger number of $6snd\ ^1D_2$ and $6snp\ ^1P_1$ Rydberg states, respectively, there are rather localized perturbations of these Rydberg series as well. Examples provide the configuration interaction of the $5d7d\ ^3F_2$ perturbing level with the $6s14d\ ^1D_2$ and 3D_2 Rydberg states (cf. Fig. 9) /18/ and the interaction of several perturbers of $5d4f$ and $5d8p\ (^3D_1, ^3P_1)$ configuration affecting $6snp\ ^1P_1$ Rydberg states below $n=16$ (cf. Fig. 8).

In the remaining part of this paper we focus our attention to the resonance in singlet-triplet mixing of $6snd\ ^1D_2$ and $6snp\ ^1P_1$ Rydberg states, caused by the $5d7d\ ^1D_2$ and $5d8p\ ^1P_1$ perturbers, respectively. For this purpose the wavefunctions of the perturbed $6snd$ Rydberg states are written as

$$|6snd\ ^1D_2\rangle = \Lambda(^1D_2) \overline{|6snd\ ^1D_2\rangle} + \Omega(^1D_2) \overline{|6snd\ ^3D_2\rangle} + \epsilon(^1D_2) \overline{|5d_{5/2}\ 7d_{3/2}\ J=2\rangle} \quad (8)$$

$$|6snd\ ^3D_2\rangle = \Omega(^3D_2) \overline{|6snd\ ^1D_2\rangle} + \Lambda(^3D_2) \overline{|6snd\ ^3D_2\rangle} + \epsilon(^3D_2) \overline{|5d_{5/2}\ 7d_{3/2}\ J=2\rangle} \quad (9)$$

with $\Lambda^2 + \Omega^2 + \epsilon^2 = 1$. The absolute phases of the wavefunctions have been chosen arbitrarily in such a way to make the largest amplitudes ($\Lambda(^1D_2)$, $\Lambda(^3D_2)$) positive. The last terms in Eqs.(8,9) account for the admixture of the doubly excited $5d7d\ ^1D_2$ state. From an analysis of the fine structure of the $5d7d$ configuration /19/ it is well known that the $5d7d$ component in the wavefunction of the $5d7d\ ^1D_2$ perturber is almost exactly *jj*-coupled corresponding to $\overline{|5d_{5/2}\ 7d_{3/2}\ J=2\rangle}$. For perturbed $6snp\ ^1,^3P$ Rydberg states, the corresponding wavefunctions can be expanded in an analogous way. Compared to the density of the $6s$ valence electron at the nucleus, the core polarization of the $5d7d$ component in the wavefunctions of perturbed $6snp\ ^1P_1$ and $6snd\ ^1D_2$ Rydberg states can be neglected. Therefore first order perturbation theory yields for the hyperfine splitting factor of perturbed $6snl\ ^1L_1$ ($l=1,2$) Rydberg states

$$A(^1L_1) = \frac{a_{6s}}{2l(l+1)} \{ \Omega^2(^1L_1) - 2\sqrt{l(l+1)} \Lambda(^1L_1) \cdot \Omega(^1L_1) \} \quad (10)$$

in complete analogy to Eq.(7). However, since $\Lambda^2 + \Omega^2 < 1$ hyperfine structure data have to be complemented by additional information, such as lifetime /20/ or isotope shift measurements /11,12/, in order to deter-

mine the amplitudes Λ, Ω and ϵ separately. It follows immediately from Eq.(10) that the sign of the measured hyperfine splitting factor A allows the relative sign of the singlet (Λ) and triplet (Ω) amplitudes to be determined.

In Figs. 10 and 11 the triplet amplitudes $\Omega(^1P_1)$ and $\Omega(^1D_2)$ have been plotted versus the principal quantum number n , respectively. Whereas hyperfine-induced mixing of $6snd\ ^1D_2$ and 3D fine structure components have been taken into account quantitatively to derive $\Omega(^1D_2)$, Eq.(10) was used to obtain preliminary values for the triplet amplitudes $\Omega(^1P_1)$ of the $6snp\ ^1P_1$ Rydberg series. It should be noted that this approximation is not valid for $6s21p\ ^1P_1$ and $6s22p\ ^1P_1$ Rydberg states. Therefore, triplet amplitudes of these states have been omitted in Fig. 10. The accuracy of the data shown in Fig. 10 is estimated to be better than 20 %. For comparison triplet amplitudes $\Omega_{th} (^1P_1)$ predicted by a multichannel quantum defect theory /15/ of the $6snp\ ^1,^3P_1$ Rydberg series are also shown in Fig. 10. As can be seen theoretical and experimental amplitudes strongly disagree. It has been shown recently /6/ that a multichannel quantum defect analysis, using term values of $6snd\ ^1,^3D_2$ Rydberg states exclusively, does not allow to derive the triplet amplitudes $\Omega(^1D_2)$ reliably. Additional

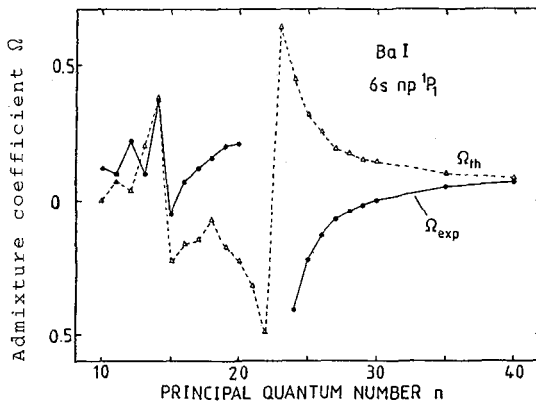
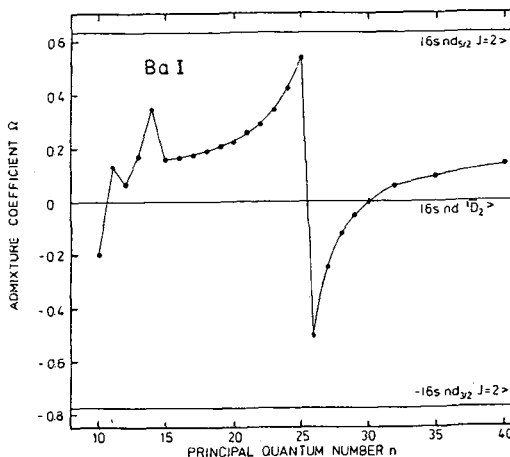


Fig. 10 - Experimental and theoretical singlet-triplet mixing parameters $\Omega(^1P_1)$ for $6snp\ ^1P_1$ states of Ba.

Fig. 11 - Experimental singlet-triplet mixing parameter $\Omega(^1D_2)$ deduced from the hyperfine structure of $6snd\ ^1D_2$ Rydberg states.



experimental data sensitive to singlet-triplet mixing, such as g-factor /10/ or hyperfine structure /7/ measurements should be used besides term values. In this way the resonance of the triplet amplitude $\Omega(^1D_2)$, (cf. Fig. 11) could be described quantitatively within a three channel model /7/. Hence the discrepancies between experimental and theoretical triplet amplitudes $\Omega(^1P_1)$ (cf. Fig. 10) call for a new multichannel quantum defect analysis of the $6snp^{1,3}P_1$ Rydberg series.

We conclude with a brief, qualitative discussion of the resonance observed for $\Omega(^1D_2)$ in the vicinity of the $5d7d^1D_2$ perturber. As can be seen from Fig. 11, this resonance is superimposed on a constant vertical offset, representing $\Omega_{so}(^1D_2)$. Therefore we express $\Omega(^1D_2)$ as

$$\Omega(^1D_2) = \Omega_{so}(^1D_2) + \Omega_{CI}(^1D_2) \quad (11)$$

and use second order perturbation theory to calculate the configuration interaction between the zero-order wavefunctions $|\overline{6snd^1D_2}\rangle$, $|\overline{6snd^3D_2}\rangle$ (cf. Eqs.(2,3)) and $|\overline{5d_{5/2}7d_{3/2}J=2}\rangle$ (cf. Eqs.(8,9)) to obtain $\Omega_{CI}(^1D_2)$. The zero-order energies, corresponding to these state vectors are denoted by $E(\overline{6snd^1D_2})$, $E(\overline{6snd^3D_2})$ and $E(\overline{5d_{5/2}7d_{3/2}J=2})$, respectively. Up to second order one obtains

$$\Omega(^1D_2) = (1 - 0.5 \epsilon_1^2) \Omega_{so}(^1D_2) + \Lambda_{so}(^1D_2) \epsilon_1 \cdot \epsilon_2 \Delta E_{TP} / \Delta E_{ST} \quad (12)$$

where

$$\Delta E_{TP} = E(\overline{6snd^3D_2}) - E(\overline{5d_{5/2}7d_{3/2}J=2}), \quad (13)$$

$\epsilon_1 = \epsilon(^1D_2)$, $\epsilon_2 = \epsilon(^3D_2)$ and the singlet-triplet separation ΔE_{ST} is given in Eq.(5). The admixture coefficients $\epsilon(^1D_2)$, $\epsilon(^3D_2)$ (cf. Eqs.(8,9)) may be obtained from second order perturbation theory. They can be expressed by the exchange integrals $R_2(6snd; 5d7d)$ and $R_2(6snd; 7d5d)$ /21/ and are inversely proportional to the perturber - Rydberg state separation. However, $\epsilon(^1D_2)$ and $\epsilon(^3D_2)$ may be taken from the three channel quantum defect analysis /7/ carried out for $6snd^{1,3}D_2$ Rydberg states in the vicinity of the $5d7d^1D_2$ perturber. It is found that the product $\epsilon_1 \cdot \epsilon_2$ stays always negative and shows a resonant behavior around $n=26,27$. Therefore the change in sign observed for $\Omega(^1D_2)$ (cf. Fig. 11) can be related to the triplet-perturber separation ΔE_{TP} (cf. Eqs.(12,13)), since the zero-order singlet-triplet splitting is always positive. Hence for Rydberg states below (above) the unshifted position of the perturber, i.e. $E(\overline{5d_{5/2}7d_{3/2}J=2})$, $\Omega_{CI}(^1D_2)$ is positive (negative). Whereas the change in sign of $\Omega_{CI}(^1D_2)$ occurs at an

energy close to the term value of the $5d7d\ ^1D_2$ perturber, for the $6snp\ ^1P_1$ series the resonance (cf. Fig. 10) is separated from the $5d8p\ ^1P_1$ perturber by about 200 cm^{-1} . Since the crossover takes place at the unshifted position of the perturber, the energy of the $5d8p\ ^1P_1$ level is raised by about 200 cm^{-1} due to its configuration interaction with the $6snp\ ^1P_1$ Rydberg states. Indeed, it is known that this perturber strongly couples to the $6snp\ ^1P_1$ series, affecting a large number of states in the discrete and continuous part of the spectrum /14,15/.

IV. CONCLUSION

Exploiting the sensitivity of thermionic detection and the considerable output powers of cw dye ring lasers, odd-parity barium Rydberg states were investigated by high resolution laser spectroscopy. Starting from the atomic ground state, the Rydberg states were reached by resonant $M1-E1$ and $E2-E1$ transitions. Generally the spectroscopy of Rydberg states populated via forbidden transitions promises to be widely applicable. From hyperfine structure and isotope shift measurements, detailed information about the electronic structure of Rydberg states can be derived.

V. ACKNOWLEDGEMENTS

This work has been supported by the Deutsche Forschungsgemeinschaft, Sonderforschungsbereich 161. The continuous interest and support of Prof. E. Matthias is acknowledged. We thank Dr. Camus for kindly communicating term values to us prior to publication. The experimental assistance of U. Majewski is acknowledged.

VI. REFERENCES

- /1/ K.C. Harvey and B.P. Stoicheff, Phys. Rev. Lett. 38, 537 (1977)
- /2/ K. Niemax and K.-H. Weber, J. Phys. B11, L267 (1978)
- /3/ E. Matthias, H. Rinneberg, R. Beigang, A. Timmermann, J. Neukammer and K. Lücke, Atomic Physics 8, Plenum Press (New York), in press
- /4/ R. Beigang, K. Lücke, and A. Timmermann, Phys. Rev. A27, 587 (1983)
- /5/ R. Beigang, E. Matthias, and A. Timmermann, Phys. Rev. Lett. 47, 326 (1981) and 48, 290 (E) (1982)
- /6/ H. Rinneberg and J. Neukammer, Phys. Rev. Lett. 49, 124 (1982)
- /7/ H. Rinneberg and J. Neukammer, Phys. Rev. A27, 1779 (1983)
- /8/ L. Barbier and R.-J. Champeau, J. Phys. (Paris) 41, 947 (1980)
- /9/ R. Menges, G. Huber, G. Ulm, and T. Köhl, to be published

- /10/ P. Grafström, C. Levinson, H. Lundberg, S. Svanberg, P. Grundevik, L. Nilsson and M. Aymar, Z. Phys. A308, 95 (1982)
- /11/ J. Neukammer, E. Matthias, and H. Rinneberg, Phys. Rev. A25, 2426 (1982)
- /12/ H. Rinneberg and J. Neukammer, J. Phys. B15, L825 (1982)
- /13/ J. Neukammer and H. Rinneberg, J. Phys. B15, 2899 (1982)
- /14/ W.R.S. Garton and F.S. Tomkins, Astrophys. J. 158, 1219 (1969)
- /15/ J.A. Armstrong, J.J. Wynne and P. Esherick, J. Opt. Soc. Am. 69, 211 (1979)
- /16/ E.R. Eliel and W. Hogervorst, Phys. Rev. A27 (1983), in press
- /17/ C. Delsart and J.-C. Keller, Opt. Comm. 15, 91 (1975)

- /18/ J. Neukammer and H. Rinneberg, J. Phys. B15, 3787 (1982)
- /19/ P. Camus, M. Dieulin, and A. El Himdy, Phys. Rev. A26, 379 (1982)
- /20/ M. Aymar, R.-J. Champeau, C. Delsart and J.-C. Keller, J. Phys. B14, 4489 (1981)
- /21/ I.I. Sobelmann, Atomic Spectra and Radiative Transitions, Springer Series in Chemical Physics Vol. 1, (Berlin, 1979)